Journal of
Plankton Research

plankt.oxfordjournals.org

J. Plankton Res. (2016) 38(2): 348–365. First published online November 30, 2015 doi:10.1093/plankt/fbv097

Costa Rica Dome: Flux and Zinc Experiments

The biological pump in the Costa Rica Dome: an open-ocean upwelling system with high new production and low export

MICHAEL R. STUKEL[1]*, CLAUDIA R. BENITEZ-NELSON[2], MOIRA DÉCIMA[3,4], ANDREW G. TAYLOR[3], CAROLYN BUCHWALD[5] AND MICHAEL R. LANDRY[3]

[1]DEPARTMENT OF EARTH, OCEAN, AND ATMOSPHERIC SCIENCE, FLORIDA STATE UNIVERSITY, TALLAHASSEE, FL 32306, USA, [2]MARINE SCIENCE PROGRAM AND DEPARTMENT OF EARTH AND OCEAN SCIENCES, UNIVERSITY OF SOUTH CAROLINA, COLUMBIA, SC 29208, USA, [3]SCRIPPS INSTITUTION OF OCEANOGRAPHY, UNIVERSITY OF CALIFORNIA AT SAN DIEGO, LA JOLLA, CA 92037, USA, [4]NATIONAL INSTITUTE OF WATER AND ATMOSPHERIC RESEARCH (NIWA), 301 EVANS BAY PARADE, HATAITAI 6021, WELLINGTON, NEW ZEALAND AND [5]WOODS HOLE OCEANOGRAPHIC INSTITUTION, WOODS HOLE, MA 02543, USA

*CORRESPONDING AUTHOR: mstukel@fsu.edu

Received April 21, 2015; accepted October 25, 2015

Corresponding editor: John Dolan

The Costa Rica Dome is a picophytoplankton-dominated, open-ocean upwelling system in the Eastern Tropical Pacific that overlies the ocean's largest oxygen minimum zone. To investigate the efficiency of the biological pump in this unique area, we used shallow (90–150 m) drifting sediment traps and ^{234}Th:^{238}U deficiency measurements to determine export fluxes of carbon, nitrogen and phosphorus in sinking particles. Simultaneous measurements of nitrate uptake and shallow water nitrification allowed us to assess the equilibrium balance of new and export production over a monthly timescale. While *f*-ratios (new:total production) were reasonably high (0.36 ± 0.12, mean ± standard deviation), export efficiencies were considerably lower. Sediment traps suggested *e*-ratios (export/^{14}C-primary production) at 90–100 m ranging from 0.053 to 0.067. ThE-ratios (^{234}Th disequilibrium-derived export) ranged from 0.038 to 0.088. C:N and N:P stoichiometries of sinking material were both greater than canonical (Redfield) ratios or measured C:N of suspended particulates, and they increased with depth, suggesting that both nitrogen and phosphorus were preferentially remineralized from sinking particles. Our results are consistent with an ecosystem in which mesozooplankton play a major role in energy transfer to higher trophic levels but are relatively inefficient in mediating vertical carbon flux to depth, leading to an imbalance between new production and sinking flux.

KEYWORDS: biogeochemistry; Eastern Tropical Pacific; plankton; carbon flux; nutrients

available online at www.plankt.oxfordjournals.org

INTRODUCTION

The Costa Rica Dome (CRD) is an open-ocean upwelling system driven by wind stress curl associated with the Papagayo wind jet (Hofmann *et al.*, 1981; Fiedler, 2002). This wind pattern causes uplift of isopycnals and a shoaling of the already shallow Eastern Tropical Pacific (ETP) thermocline in the region of 9°N, 90°W, which introduces new nutrients into the euphotic zone and stimulates primary production. Uniquely among upwelling systems, nutrient input to the CRD leads to a community dominated by cyanobacteria, particularly *Synechococcus* (Li *et al.*, 1983; Saito *et al.*, 2005). At the same time, however, the CRD appears to support large communities of mesozooplankton (Fernandez-Alamo and Farber-Lorda, 2006) and high biomasses of higher trophic levels (e.g. whales and seabirds, Reilly and Thayer, 1990; Vilchis *et al.*, 2006).

The CRD overlies one of the largest oxygen minimum zones (OMZs) in the world. Productivity in the CRD contributes to the OMZ by supplying a steady rain of sinking organic matter. At the same time, low oxygen content of the OMZ likely retards remineralization of sinking particulate material, enhancing gravitational transport of particles (hereafter, export) to depth (Van Mooy *et al.*, 2002). The CRD is therefore an ecosystem in which efficient transport of particulate carbon (PC) and particulate nitrogen (PN) to depth is hypothesized to balance the input of new nitrogen by upwelling. However, the prevalence of small phytoplankton also suggests a system with decreased export efficiency, as smaller particles sink more slowly and are subject to increased remineralization losses (Michaels and Silver, 1988).

The CRD is thus an interesting region in which to assess whether the export of sinking particles balances new production, defined (following Eppley and Peterson, 1979) as production based on allochthonous sources of nitrogen, coming primarily as upwelled nitrate from nutrient-rich deep waters. This assumed balance between new and export production has been a cornerstone of marine biogeochemistry, but has seldom been directly assessed in marine ecosystems due to the difficulty of conducting studies over sufficiently large spatial and long temporal scales with complementary methods. One such study in the Equatorial Pacific, an open-ocean upwelling system with similarities to the CRD, during the JGOFS program featured spring and fall survey and time-series cruises on which both nitrate uptake and export (sediment traps, ^{234}Th disequilibrium) were measured. In summarizing these and other carbon flux results, Quay (Quay, 1997) found a carbon balance for the spring survey cruise during which export was ~60% of new production (Buesseler *et al.*, 1995; McCarthy *et al.*, 1996). However, if NO_3^- uptake measurements from the time-series cruise were used instead (Bacon *et al.*, 1996), export accounted for only ~20% of new production, resulting in a carbon imbalance. In the fall, new production was high and export measurements varied substantially based on the methodology, resulting in balanced carbon budgets if the highest carbon export estimate was used (~70% of new production, Murray *et al.*, 1996), but unbalanced budgets if the two lower carbon export estimates were used (~8 or 15% of new production, Buesseler *et al.*, 1995; Wakeham *et al.*, 1997). The inability to truly balance new and export production not only points to issues with current methods (Burd *et al.*, 2010) but also suggests that processes other than export may be contributing to carbon removal from open-ocean systems.

As part of the FLUZiE (Flux and Zinc Experiments) cruise in July 2010, we focused on the biological pump in the CRD, to determine whether export efficiency from this unique and productive region followed expectations for an upwelling region (high export efficiency) or for a picoplankton-dominated ecosystem (low efficiency). We measured sinking particle export using a combination of ^{238}U:^{234}Th disequilibrium and free floating sediment traps. Carbon, nitrogen and phosphorus stoichiometry as well as carbon and nitrogen isotopes within sediment trap material were determined to assess sources and composition. Using a Lagrangian sampling plan to assess non-steady-state issues, we also measured nitrate uptake, nitrification and nitrogen export rates in the same water parcels to test whether we could resolve a balance between new and export production for the CRD ecosystem. Our measurements provide the first direct assessment of particulate organic fluxes from the euphotic zone to the upper oxygen-deficient waters of the CRD and the first attempt to integrate carbon pump parameters into an ecological study of plankton dynamics in the region. Our results suggest that during our study gravitational export of sinking particles and aggregates only accounts for a small fraction of new production. Although this imbalance may result from longer timescale variability in upwelling, nitrate uptake and export production, ancillary measurements do not support the supposition that the ecosystem was experiencing a pulse of enhanced new production during our study period. Rather, ecosystem rate measurements suggest that the CRD was in a state of transient equilibrium featuring food web processes that efficiently shunt organic matter through mesozooplankton to higher trophic levels, thus decreasing the proportion of total ecosystem export attributable to gravitational flux. Conclusively, testing the equivalence of new production and particle export requires year-long measurements on a regional scale that are beyond the realistic scope of open-ocean research

programs. However, we believe that smaller scale Lagrangian approaches like ours offer a tractable approach for examining the balance of new and export production over shorter timescales and point to other important pathways for carbon loss in upwelling dominated ecosystems.

METHOD

Cruise plan

The CRD FLUZiE cruise was conducted on *R/V Melville* from 23 June to 24 July 2010 with a sampling plan based on multi-day semi-Lagrangian experiments. In each of five experimental "cycles," we used satellite-tracked drifting buoys with attached drogues centered at 15-m depth to follow water parcels for three (Cycle 1) or four (Cycles 2–5) days as we measured plankton community dynamics and biogeochemical fluxes (Landry *et al.*, 2009; Stukel *et al.*, 2013a). Attached to each floating array was either a suite of sediment traps at two depths or eight mesh bags containing experimental incubation bottles at depths spanning the euphotic zone (see Landry *et al.*, 2016a). These Lagrangian cycles allowed us to simultaneously measure vertical fluxes (sediment traps and ^{234}Th:^{238}U disequilibrium), phytoplankton production ($^{15}NO_3^-$ and $H^{14}CO_3^-$ uptake), nutrient concentrations, standing stocks [pigments, suspended particulate organic carbon (POC), suspended PN, isotopic composition of suspended particulates] and net *in situ* rates of change of particular organic material (POM) and the phytoplankton community. Cycle 1 was initiated in a coastal region inshore of the CRD (Fig. 1). Cycle 2 began in the central core area of the CRD, and Cycle 4 was initiated at the location of a drifter that had been left for 5 days at the site of the end of Cycle 2. The remaining Cycles 3 and 5 were initiated in waters slightly west and east of the

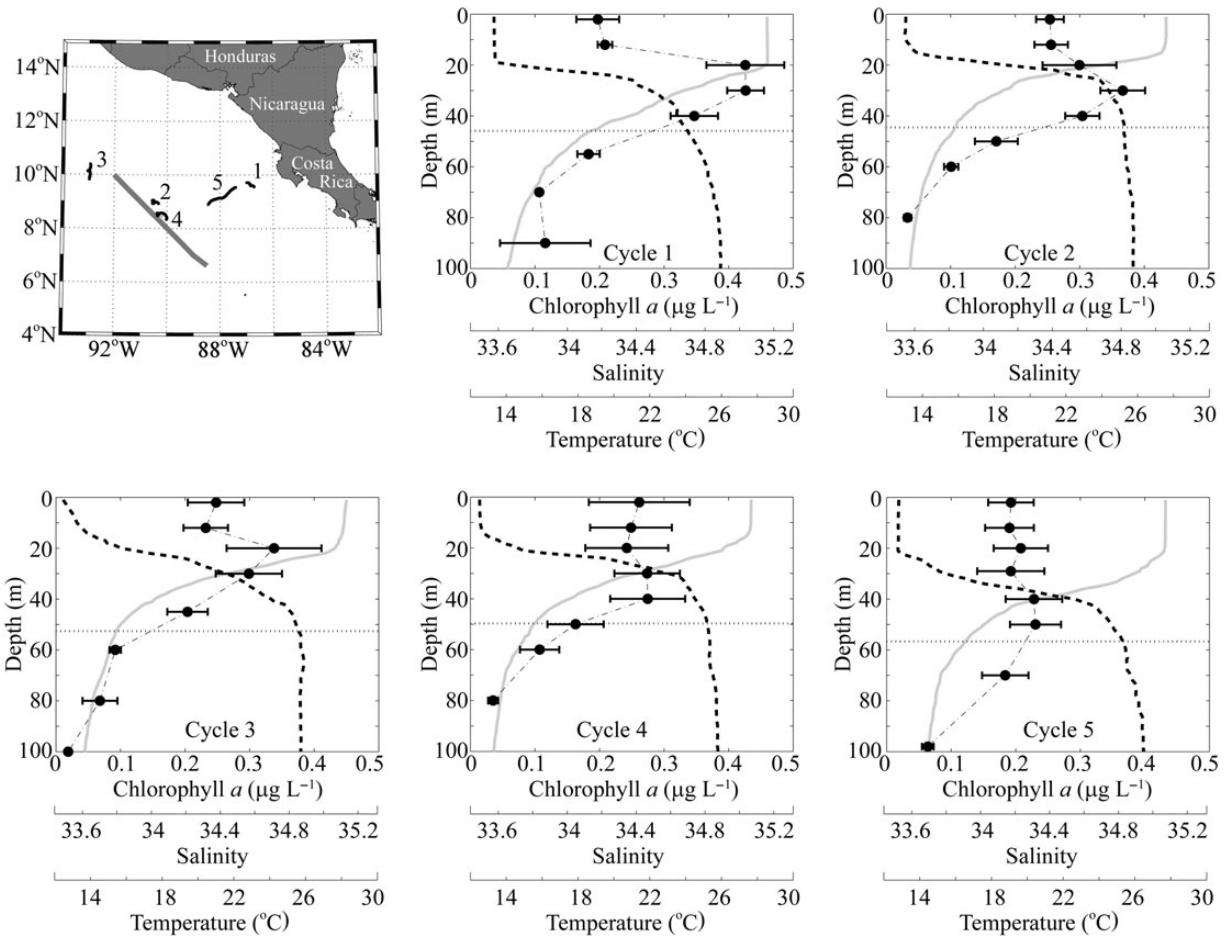

Figure 1. Cruise overview. Upper left panel shows CRD study region in the Eastern Tropical Pacific. Thick, straight gray line is our transect across the CRD. Curved black and gray lines are the experimental array and sediment trap drifter tracks, respectively. Note that sediment trap tracks are seldom visible at this scale, because the drifters stayed closely together. Numbers label the individual cycles. All other panels show mean Chl *a* (black circles and dashed-dotted line), salinity (solid gray line) and temperature (black dashed line) depth profiles for the cycles. For Chl *a*, error bars show the standard error. Horizontal dotted line is depth of the 1% light level.

core of the CRD, respectively. A >500-km transect through the CRD, sampled between Cycles1 and 2, allowed us to determine large-scale patterns in biogeochemical properties.

Sediment trap deployments

The sediment trap array was deployed at the beginning and recovered at the end of each experimental cycle. The array included satellite drifter, drogue and two VERTEX-style particle interceptor tube crosspieces (Knauer *et al.*, 1979; Stukel *et al.*, 2013a), deployed at the base of the Chl-containing layer (100 m on Cycle 1, 90 m on other cycles and at 150 m). Each crosspiece held 8–12 trap tubes, with a baffle of smaller tapered tubes. Tubes were deployed with 2 L filtered seawater slurry (50 g L^{-1} NaCl and 1% formalin). Upon recovery, samples were filtered through a 200-μm filter and mesozooplankton swimmers were removed from the filter contents. Samples were split on a rotary splitter for POC, inorganic C, PN, $PO^{13}C$, $P^{15}N$, element:^{234}Th ratio, total P, organic P, pigments and microplankton biomass analyses (the latter two reported in Stukel *et al.*, 2013a). All samples were then filtered through pre-combusted GF/F filters, except samples for element:^{234}Th ratio measurements, which were filtered through pre-combusted quartz filters. See Supplementary data, for more details.

^{234}Th Measurements

Samples (4 L) for analysis of water column ^{234}Th concentrations were typically taken at 12 depths spanning the upper 150 m on two casts per experimental cycle. On two cycles in the core of the CRD, an additional set of 8 samples was taken to assess ^{234}Th deficiency down to 500-m depth. Samples were analyzed by standard small-volume procedures (Benitez-Nelson *et al.*, 2001; Buesseler *et al.*, 2001; Pike *et al.*, 2005), including a ^{230}Th yield tracer spike, co-precipitation with manganese oxide, beta counting on a RISO beta multi-counter and yield analyses by ICP-MS. ^{234}Th export was determined by vertically integrating ^{234}Th and ^{238}U activities and applying a 1D steady-state equation: Export $= \lambda_{234}(^{238}U - {}^{234}Th)$, where λ_{234} is the ^{234}Th decay constant. To estimate sinking POC and PN flux from ^{234}Th export, we measured element:^{234}Th ratios on sinking particles collected by sediment traps and >50-μm particles sampled with an *in situ* pump. Total particulate P (TPP) and particulate inorganic P (PIP) were determined on one sediment trap sample from all trap depths using a modification of the Aspila phosphomolybdate method (Aspila *et al.*, 1976; Benitez-Nelson *et al.*, 2007). See Supplementary data, for more details.

POC, PN and isotopic analyses

Samples were collected at eight depths from two casts per cycle for upper ocean suspended POC, suspended PN and C and N isotopic analyses. Samples were filtered onto pre-combusted GF/F filters and frozen in liquid N_2. Samples were subsequently acidified and analyzed by mass spectrometer. Two sediment trap samples from the shallowest trap depth at each cycle were similarly prepared and analyzed. An additional 3–5 GF/F samples for each trap depth were cut in half, with only half of the filter acidified. Both halves were analyzed to determine sinking POC (and PN flux), total PC flux and (by difference) particulate inorganic carbon fluxes. See Supplementary data, for more details.

Primary productivity and new production

$^{15}NO_3$ and $H^{14}CO_3^-$ uptake rates were determined daily from samples incubated on our *in situ* array at eight depths. Nitrate uptake samples were spiked with $K^{15}NO_3$ (0.1 μmol L^{-1}), and primary productivity (^{14}C-PP) samples were spiked with $H^{14}CO_3$. All samples were incubated *in situ* for 24 h beginning and ending at ~0400 local time. Nitrate uptake was calculated following Dugdale and Wilkerson (Dugdale and Wilkerson, 1986).

In addition to 24-h incubations, we conducted three diel experiments in deck incubators screened to 33% surface irradiance to approximately match mixed-layer light levels. For each experiment, eight 1.2-L bottles were filled. Two control bottles were spiked with $^{15}NO_3$ and incubated for 24 h. The remaining six bottles were sequentially spiked and filtered every 4 h, thus giving a time-series of 4-h incubations to compare to the 24-h incubation control bottles.

The assumption that nitrate uptake is representative of true new production has been challenged by studies demonstrating measurable rates of nitrification in surface waters (Dore and Karl, 1996; Yool *et al.*, 2007). To assess the fraction of nitrate uptake that represented true new production (production based on nitrogen introduced to the surface ocean by upwelling and/or mixing), we measured nitrification rates at two depths in the euphotic zone on Cycles 2–4, by incubating natural water with labeled $^{15}NH_4^+$ and measuring the production of $^{15}NO_2^-$ and $^{15}NO_3^-$ by the denitrifier method (Sigman *et al.*, 2001; Buchwald *et al.*, in revision). New production was determined by subtracting vertically integrated shallow water nitrification rates from vertically integrated nitrate uptake rates. We computed *f*-ratios (fraction of total phytoplankton supported by new production) by dividing new production by ^{14}C-PP converted to nitrogen units using a Redfield C:N ratio of 6.625. We chose to use this canonical ratio rather than a ratio derived from our

POC:PN measurements because non-living detritus often comprises a majority of POM (Riley, 1970; Yanada and Maita, 1995). However, this canonical ratio was not significantly different from our measured POC:PN ratio of 6.3 ± 1.1. See Supplementary data, for more details. Unless otherwise noted, all values in this manuscript are means ± standard deviations.

RESULTS

Cruise conditions

The CRD was sampled during mild El Niño conditions, when the dome structure was less sharply defined, sea-surface chlorophyll was decreased compared with the climatological mean (Landry *et al.*, 2016a), and *Synechococcus* concentrations, while still quite high (Selph *et al.*, 2016), were much lower than reported from previous cruises in the region (Li *et al.*, 1983; Saito *et al.*, 2005). A strong thermocline was found between 20 and 40–60 m depth, separating 28–29°C surface water from <18°C water below (Fig. 1). The 20°C isotherm (25, 33, 32 and 41 m for Cycles 2–5) was deeper than the climatological mean for summer (Fiedler and Talley, 2006), suggesting reduced upwelling. The thermocline was associated with a nitracline that shoaled from 35 m in our furthest inshore experiment (Cycle 1) to 20 m in the core of the dome. Surface Chl *a* ranged from 0.2 to 0.3 μg Chl *a* L^{-1}, and a weak chlorophyll maximum was observed in three of the five cycles just below the base of the mixed layer. Across the transect, oxygen concentrations decreased substantially in the thermocline from surface concentrations of >200 μmol kg^{-1} to concentrations an order of magnitude lower at depths below 80 m (Supplementary data, Fig. S1). Light attenuation was higher than in most open-ocean regions, with euphotic zone depths (defined as the 1% light level) averaging 50 m (Goes *et al.*, 2015) and >90% of ^{14}C-derived phytoplankton primary production occurring in the upper 40 m.

POC and PN profiles were similar in all offshore cycles (Cycles 2–5), but markedly different during the nearshore Cycle 1 (Fig. 2). POC concentrations decreased gradually from surface concentrations in the range of 8–16 μmol C L^{-1} to concentrations of ~ 4 μmol C L^{-1} below 80 m depth. The C:N ratio of sinking material increased with depth. Surface waters showed molar ratios slightly below the canonical Redfield values of 6.625 (C:N), while values below the euphotic zone increased steadily for all offshore cycles to >7.9. δ^{13}C of POC in the surface ocean averaged −21‰ and decreased significantly in the thermocline before leveling out below the thermocline at values of −26 to −25‰. The δ^{15}N of POM showed a more complicated pattern, decreasing slightly in the thermocline, rising beneath the thermocline and then potentially decreasing again at depths greater than 80 m. Surface waters were not depleted in PO^{15}N as would have been expected if dinitrogen fixation rates were substantial. Because of the strong differences in location, physics, biogeochemistry and plankton communities between Cycle 1 (nearshore) and the other cycles closer to the CRD core (Landry *et al.*, 2016a), all CRD means reported in this manuscript refer only to Cycles 2–5.

Nitrate uptake

Diel $^{15}NO_3$ uptake experiments, conducted on Cycles 1, 3 and 4, confirmed that 24-h incubations were not underestimating nitrate uptake as a result of nitrate depletion during the incubation. The average rates determined from 4-h incubations closely matched rates from

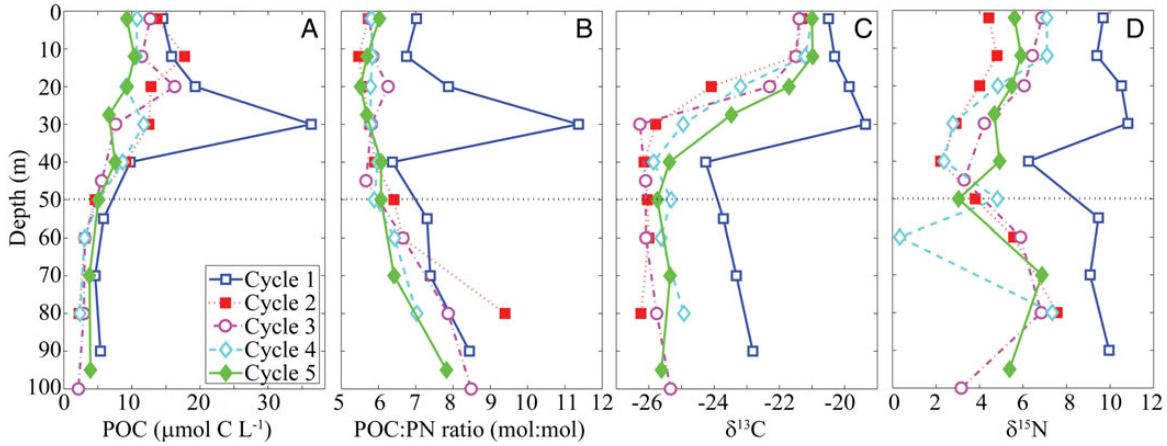

Figure 2. Particulate organic material (POM) on five experimental cycles. Each profile is the mean of measurements taken on the first and last CTD cast of the cycle. Panel **A** shows particulate organic carbon (POC) concentrations. Panel **B** shows ratio of POC to particulate nitrogen (PN). Panels **C** and **D** show carbon and nitrogen isotopic content of POM, respectively. Horizontal dotted line is depth of the 1% light level.

simultaneous 24-h incubations. The diel experiments consistently showed enhanced daytime nitrate uptake, with peak daytime rates exceeding the daily means by factors of 2.5–3.2 (Fig. 3). These high day:night ratios of nitrate uptake suggest that phytoplankton were not nitrogen limited (Mulholland and Lomas, 2008), a result that is consistent with nutrient-amended grow-out experiments on the cruise (Goes *et al.*, 2015).

Vertical profiles of *in situ* ^{14}C primary production (^{14}C-PP) showed low intraregional variability, with mean vertically integrated values of 87 mmol C m^{-2} day^{-1} (range 83–100 mmol C m^{-2} day^{-1}), and consistent surface productivity enhancement. By comparison, NO_3^- uptake values were more variable (CRD mean 8.6 mmol N m^{-2} day^{-1}, range 4.8–17.7 mmol N m^{-2} day^{-1}, Fig. 4). NO_3^- uptake rates were enhanced at the surface for Cycles 1, 2 and 4, but showed little vertical structure for Cycles 3 and 5. Surface *f*-ratios, based on assumed Redfield C:N molar uptake ratios of 6.625:1, were typically in the range of 0.2–0.4 in the upper euphotic zone, but substantially >1.0 beneath the nitracline. Bulk plankton nitrate uptake rates thus exceeded the Redfield nitrogen requirement of phytoplankton below the euphotic zone (~50 m). Assuming that *f*-ratios >1 were indicative of luxury uptake or uptake by non-phytoplankton, we can calculate a conservative NO_3^- uptake rate (minimum of NO_3^- uptake and ^{14}C-PP/6.625) for each

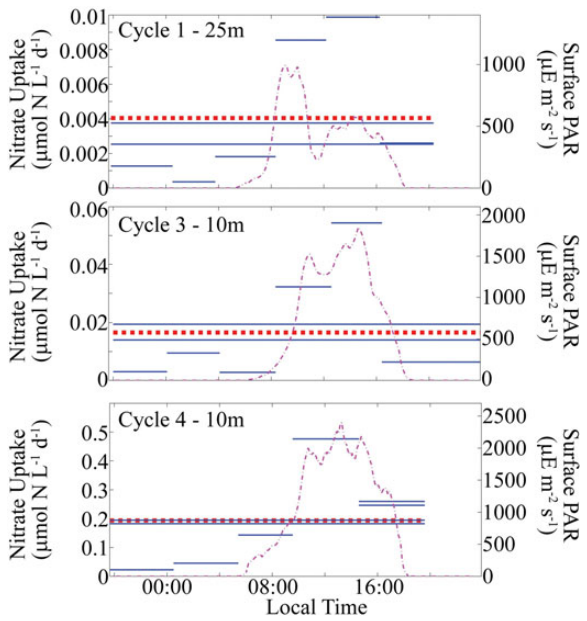

Figure 3. Results of diel nitrate uptake experiments conducted on shipboard. Solid horizontal lines show the duration and mean uptake rate for 4–5 h and 24-h incubations. Dashed horizontal line shows mean of short incubations for comparison with the 24-h incubations carried out at the same time. Dashed-dotted lines show surface photosynthetically active radiation (PAR).

experiment (except Cycle 1 when ^{14}C-PP was not measured). By this more conservative metric, vertically integrated nitrate uptake (from surface to 80 to 100 m depth) averaged 4.8 mmol N m^{-2} day^{-1} (range: 3.1–7.2 mmol N m^{-2} day^{-1}). While surface nitrate values through most of the region exceeded 1 μM, mixed-layer values for Cycle 1 averaged 0.1 μM. Thus, our NO_3^- uptake measurements for this cycle (with a spike of 0.1 μM $^{15}NO_3^-$) may have been biased.

Vertically integrated nitrification rates for Cycles 2–4 were 69.2 ± 19.6, 7.6 ± 0.9 and 19.2 ± 0.6 μmol NO_3^- m^{-2} day^{-1}, respectively. Given the high nitrate concentrations beneath the mixed layer, this would suggest very high residence times for NO_3^- with respect to nitrification. Since even our conservative measured nitrate uptake rates (mean of 4.8 mmol N m^{-2} day^{-1}) were 2–3 orders of magnitude greater, we argue that our nitrate uptake assessments of new production were not confounded by nitrification within the euphotic zone.

To compare the roles of different phytoplankton size-classes in nitrate uptake, we regressed nitrate uptake with the production of picoplankton and larger phytoplankton. Picoplankton production rates for *Synechococcus, Prochlorococcus* and picoeukaryotic phytoplankton were determined from growth and grazing rates of dilution experiments assessed via flow cytometry (Selph *et al.*, 2016; Landry *et al.*, 2016b), while nano-microplankton production was assessed by the difference between ^{14}C-PP and picoplankton production. While no statistically significant correlation was found between picoplankton and nitrate uptake ($r^2 = 0.004$, Supplementary data, Fig. S2), a strong positive correlation was found between nitrate uptake and nano-microplankton production ($r^2 = 0.50$; Supplementary data, Fig. S2).

^{234}Th Measurements

^{234}Th was consistently depleted relative to ^{238}U in surface waters (Fig. 5). Surface deficiencies decreased with depth over the upper 40 m before reaching equilibrium with ^{238}U near the base of the euphotic zone (1% light level averaged 50 m). Using a 1D steady-state approximation, ^{234}Th export fluxes at the 90 m depth horizon (or 100 m for Cycle 1) were greatest for Cycles 1 and 5 (2117 ± 108 and 1546 ± 201 dpm m^{-2} day^{-1}, respectively). ^{234}Th export was lower in the core of the dome (1030 ± 188 and 851 ± 153 dpm m^{-2} day^{-1} for Cycles 2 and 4, respectively) and in the offshore Cycle 3 (651 ± 197 dpm m^{-2} day^{-1}). Export fluxes at 150-m depth showed similar inter-cycle patterns (2222 ± 204 and 1588 ± 303 dpm m^{-2} day^{-1}for Cycles 1 and 5, respectively; 945 ± 296 and 882 ± 266 dpm m^{-2} day^{-1}

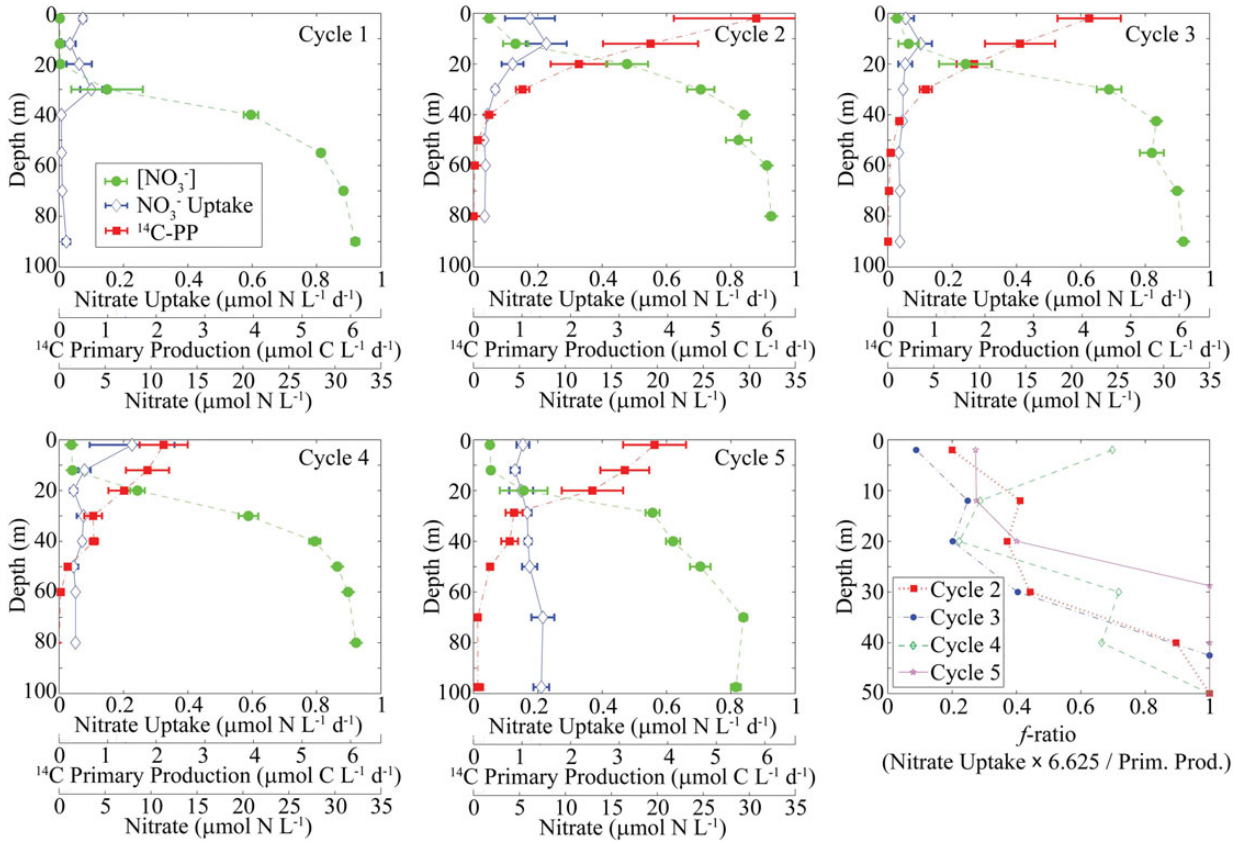

Figure 4. $^{15}NO_3^-$ and $H^{14}CO_3^-$ uptake. In the first five panels, open diamonds are $^{15}NO_3^-$ uptake measurements, solid black squares are $H^{14}CO_3^-$ uptake and solid gray circles are NO_3^- concentrations. Note that $^{15}NO_3^-$ uptake and $H^{14}CO_3^-$ uptake axes are scaled such that equal values would equate to an *f*-ratio of 1, assuming Redfield (6.625 molar ratios of C:N). Error bars are replicate measurements made over the course of the cycle. Bottom right panel shows *f*-ratio assuming Redfield C:N uptake in the euphotic zone. *f*-ratios are capped at 1.

for Cycles 2 and 4, respectively and 651 ± 279 dpm m^{-2} day^{-1} for Cycle 3).

To convert steady-state ^{234}Th export measurements to carbon export, we measured the C:^{234}Th ratio of POM collected using both sediment traps and *in situ* pumps. C:^{234}Th ratios were consistently higher in sediment trap particles (5.8 ± 3.3 μmol C dpm^{-1} at 150 m) than in the >50-μm particles collected with *in situ* pumps (Table I, Supplementary data, Fig. S3, Sediment Trap C:Th > Pump C:Th with paired one-sided *t*-test $P = 0.019$). There was also a significantly lower C:^{234}Th ratio for <200-μm particles compared with >200-μm particles collected by the sediment traps (paired one-sided *t*-test $P = 0.037$). Smaller particles had a relatively invariant C:^{234}Th ratio (150 m = 3.4 ± 0.9 μmol C dpm^{-1}, range 2.6–3.9), while the >200-μm particles had significantly higher and more variable C:^{234}Th ratios of 41.5 ± 60.3 μg C dpm^{-1} (range 4.9–131.2). The C:^{234}Th ratios of swimming mesozooplankton removed from the sediment traps were much higher than for sinking particles, ranging from 350 to 1028 μmol C dpm^{-1} at 150 m (these swimmers are not included in calculations of overall C:^{234}Th ratios of sinking particles collected by traps). N:^{234}Th ratios of particulate matter followed similar patterns (N:$^{234}Th_{zooplankton}$ > N:$^{234}Th_{largesinking}$ > N:$^{234}Th_{smallsinking}$) and averaged 0.67 ± 0.34 μmol N dpm^{-1} for bulk sinking material at the shallow trap depth, decreasing to 0.614 ± 0.24 μmol N dpm^{-1} at 150 m. Because of the relatively good collection efficiency (^{234}Th measurements suggest that sediment traps were over-collecting by ~19%, see Discussion) of the sediment traps (trap material is likely more representative of sinking material than pump samples) and the fact that sediment traps were consistently deployed at similar depths on all cycles, we used sediment trap element:^{234}Th ratio to estimate ^{234}Th-based carbon and nitrogen export. This provides maximum estimates of POC and PN export rates, relative to results using the lower element:^{234}Th ratios from the pump samples.

^{234}Th-based estimates at the 90–100 m depth horizon suggest relatively high export for coastal Cycle 1 (24.5 ± 4.8 mmol C m^{-2} day^{-1}), but low-to-moderate export

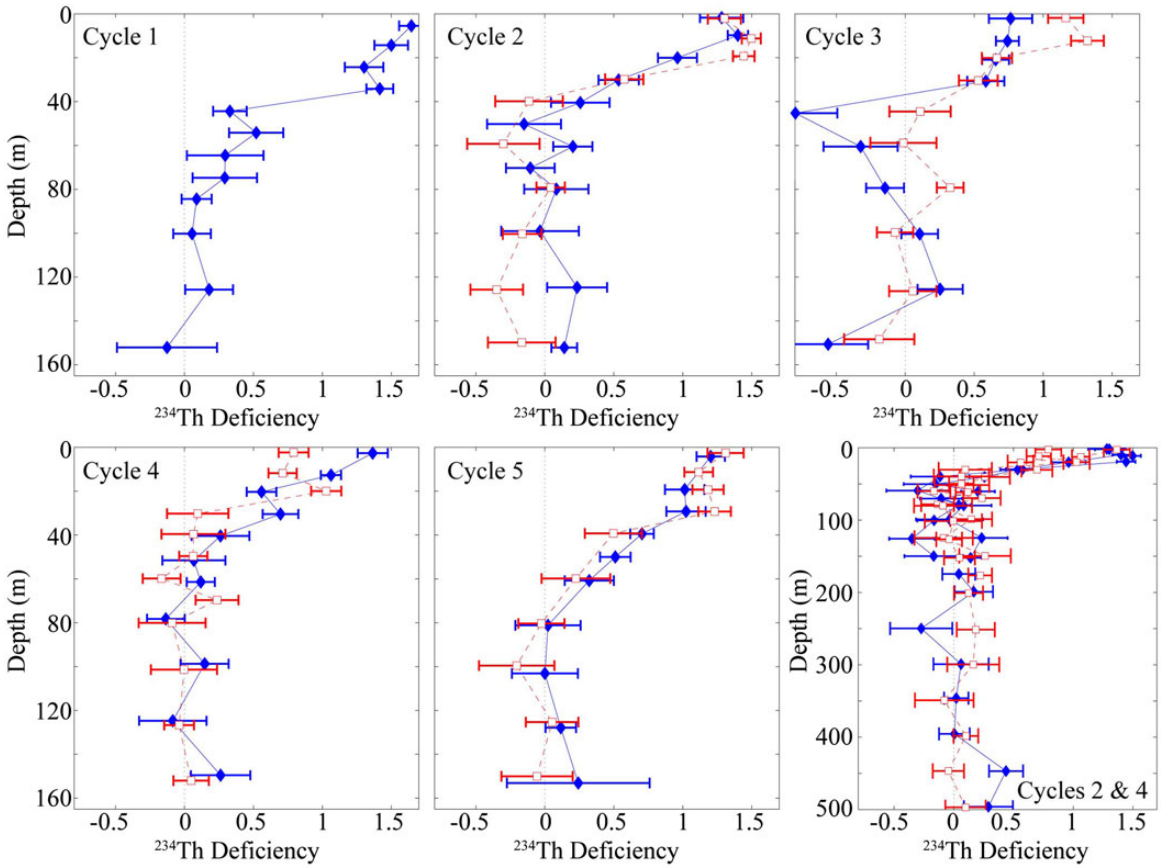

Figure 5. Thorium deficiency profiles. First five panels show ^{238}U-^{234}Th deficiencies for the epipelagic for each cycle (positive values indicate thorium deficit and are indicative of export). All cycles except Cycle 1 show a profile at the beginning (filled diamonds) and end (open squares) of the 4-day cycle. Bottom right panel shows ^{238}U-^{234}Th deficiency in the mesopelagic for Cycle 2 (filled diamonds) and Cycle 4 (open squares) in the core of the dome. In all panels, error bars are propagation of measurement uncertainty.

rates for Cycles 2–5 (8.8 ± 1.8, 3.2 ± 3.2, 3.1 ± 1.0 and 5.7 ± 0.7, respectively). ^{234}Th results showed no statistically significant differences in POC flux between the shallow (90 or 100 m) and deep (150 m) trap depths, implying little remineralization between the two depth horizons. The low remineralization rates may be tied to low oxygen concentrations; dissolved oxygen dropped to <20 μmol O_2 kg^{-1} deeper than ~50 m for the cycles closest to the core of the CRD (Supplementary data, Fig. S4).

Sediment trap measurements

Sediment trap POC flux measurements for CRD cycles (Cycles 2–5) averaged 5.3 ± 0.8 mmol C m^{-2} day^{-1} at our shallow trap depth and 4.4 ± 0.6 mmol C m^{-2} day^{-1} at 150 m (Table II). POC flux measurements were not significantly different from total particulate carbon (PC_{tot}) flux measurements (mean PC_{tot} flux at shallow trap depth was 5.4 ± 1.0 mmol C m^{-2} day^{-1}; for 150-m traps flux was 4.6 ± 0.7 mmol C m^{-2} day^{-1}), suggesting that $CaCO_3$ was not a significant component of the sinking material. POC vertical flux was highest in our inshore Cycle 1 (10 ± 0.7 mmol C m^{-2} day^{-1} at 100 m). It was slightly depressed in the core of the dome (5.3 ± 1.5 and 4.2 ± 0.6 mmol C m^{-2} day^{-1} at 90 m for Cycles 2 and 4, respectively) relative to the surrounding regions (5.6 ± 0.4 and 6.0 ± 0.5 mmol C m^{-2} day^{-1} at 90 m, for Cycles 3 and 5, respectively). The mean sediment trap-derived POC flux attenuation in the depth horizon between our traps was 0.2% m^{-1}, equating to average remineralization of 13% of POC over the 50–60 m separating the two traps. POC residence time in the surface ocean (with respect to sinking) averaged 4 months, with relatively low inter-cycle variability (min = 96 days, max = 144 days).

C:N molar ratios of sinking material averaged 10.0 at our shallow trap depth, increasing to 11.4 at 150 m. Both ratios were significantly higher than the mean C:N molar ratios of POM suspended in the mixed layer, suggesting preferential nitrogen remineralization. Similarly, N:P and C:P molar ratios (26 and 262, respectively at our shallow trap depth; 26 and 287, respectively at 150 m) exceeded

Table I: C:^{234}Th ratio (μmol C dpm^{-1}) collected by McLane WTS-LV in situ *pump (*is*Pump) with >50-μm Nitex screen, sediment trap, sediment trap <200-μm material (ST <200), sediment trap >200-μm material (ST >200) and swimming mesozooplankton that were removed from the sediment trap (Mesozoo)*

Cycle	Depth	*is*Pump	SedTrap	ST <200	ST >200	Mesozoo
1	100	4.2 ± 0.9	11.6 ± 2.3	5.4 ± 0.7	39.8	518.1
1	150		9.4 ± 1.1	4.6 ± 0.6	34.7	371.6
2	30	3.8				
2	90	3.4 ± 0.1	8.5 ± 1.4	3.9 ± 0.2	53.1	384.9
2	150		10.2 ± 1.1	4.6 ± 0.1	131.2	350.2
2	400	1.8				
3	90		4.9 ± 0.4	3.7 ± 0.3	8.9 ± 2.1	50.4
3	150	3.1	6.2 ± 0.9	3.3 ± 0.4	22.4	461.1
4	90	2.4 ± 0.3	3.7 ± 0.4	3.2 ± 0.4	5.7 ± 0.3	172.6
4	150		3.6 ± 0.3	3.1 ± 0.1	7.6 ± 0.6	
4	400	1.6				
5	90	2.6	3.7 ± 0.5	2.9 ± 0.4	5.3 ± 0.3	69.4
5	150	2.7	3.1 ± 0.6	2.6 ± 0.2	4.9 ± 0.3	1027.6

Values are mean ± standard deviation of replicate measurements (unless no replicates were collected).

Table II: Mass fluxes into shallow drifting sediment traps: particulate organic carbon (mmol C m^{-2} day^{-1}), particulate nitrogen (mmol N m^{-2} day^{-1}), total particulate phosphorus (μmol m^{-2} day^{-1}), particulate inorganic phosphorus (μmol m^{-2} day^{-1}), particulate organic phosphorus (μmol m^{-2} day^{-1}), organic carbon:nitrogen ratio (mol:mol), nitrogen:total phosphorus ratio (mol:mol), δ^{15}N (‰), δ^{13}C (‰)

Cycle	Depth	POC	N	TPP	PIP	POP	C:N	N:P	δ^{15}N	δ^{13}C
1	100	10 ± 0.7	0.9 ± 0.11	34.8 ± 2.7	8.8 ± 2.5	26.0 ± 4.3	11.2	25.7	8.7 ± 0.02	−21.0 ± 0.4
1	150	9.3 ± 1.3	0.76 ± 0.1	24.8	8.0	16.8	12.2	30.7		
2	90	5.3 ± 1.5	0.53 ± 0.11	19.1 ± 2.3	4.0 ± 0.1	15.2 ± 2.1	10.1	27.6	14.3 ± 9.1	−24.1 ± 1.6
2	150	4.2 ± 0.6	0.47 ± 0.06	12.8 ± 1.7	4.6 ± 1.3	8.2 ± 0.3	9.1	36.1		
3	90	5.6 ± 0.4	0.55 ± 0.05	18.7 ± 3.6	6.2 ± 1.8	12.6 ± 5.3	10.2	29.4	4.6 ± 3.6	−24.4 ± 0.10
3	150	4.6 ± 0.2	0.35 ± 0.02	19.9 ± 6.4	7.8 ± 1.4	12.0 ± 7.8	13.3	17.4		
4	90	4.2 ± 0.5	0.4 ± 0.04	15.9 ± 0.1	6.9 ± 1.3	9.0 ± 1.3	10.4	25.4	5.3 ± 1.7	−24.0 ± 0.03
4	150	3.8 ± 0.3	0.34 ± 0.04	11.9 ± 1.1	5.7 ± 0.3	6.2 ± 0.9	11.4	28.2		
5	90	6 ± 0.5	0.64 ± 0.07	29.3 ± 3.9	6.8 ± 2.1	22.5 ± 1.9	9.5	21.8	6.9 ± 0.6	−24.1 ± 0.2
5	150	5.1 ± 0.3	0.43 ± 0.03	19.4 ± 1.9	7.0 ± 1.1	12.4 ± 1.1	12.0	22.2		
Mean	90/100	5.3	0.53	20.8	6	14.8	10.0	26.0	7.8	−24.2
Mean	150	4.4	0.4	16	6.3	9.7	11.4	26.1		

Bottom two rows are means of dome-related cycles (2–5). Mean ± standard deviation.

Redfield, indicating preferential remineralization of phosphorus. Organic phosphorus comprised roughly two thirds of total sinking phosphorus.

While the stoichiometric ratio of the sinking material suggested that organic matter was significantly reworked and preferentially remineralized as it sank, δ^{15}N signatures of the sinking material showed no consistent pattern relative to euphotic zone PN. δ^{15}N signatures for most cycles were relatively similar to the δ^{15}N of surface POM. For Cycle 2, the sediment trap δ^{15}N was substantially higher; however, this resulted from 1 sample with a δ^{15}N of 7.9 and another of 20.8. For Cycles 2–5, the δ^{13}C of sinking POC was consistently depleted relative to surface POC (-24.2 ± 0.1 for sinking material; -21.2 ± 0.2 for surface POC, $P < 0.001$). The sinking POM, however, was enriched in ^{13}C relative to suspended material at the same depth ($P = 0.015$).

Comparison of new production and gravitational sinking flux

Sediment trap and steady-state ^{234}Th results both suggest that gravitational nitrogen flux out of the upper water column was relatively low. Sediment traps provided mean nitrogen flux estimates across CRD cycles of 0.53 ± 0.10 mmol N m^{-2} day^{-1} (range 0.40–0.64) at 90–100 m and 0.40 ± 0.64 mmol N m^{-2} day^{-1} (range 0.34–0.43) at 150 m. For comparison, ^{234}Th results suggested mean nitrogen flux of 0.79 ± 0.47 mmol N m^{-2} day^{-1} (range 0.37–1.21) at 90–100 m and 0.66 ± 0.19 mmol N m^{-2} day^{-1} (range 0.37–0.76) at 150 m.

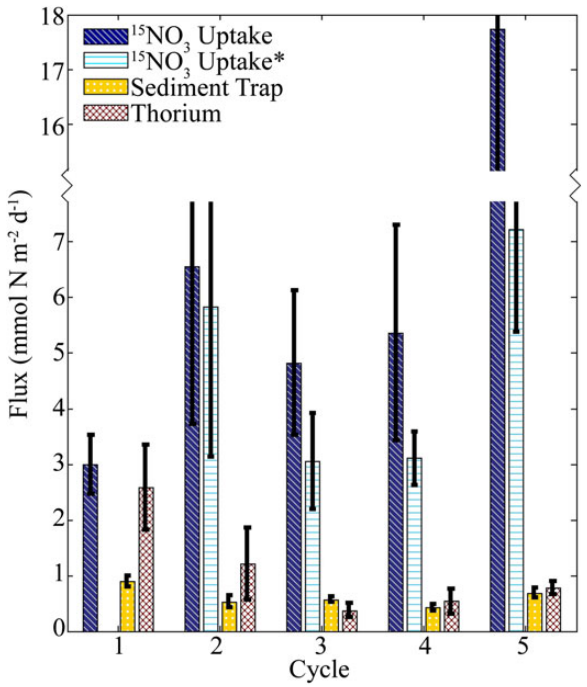

Figure 6. Comparison of nitrate uptake and vertical nitrogen flux. $^{15}NO_3^-$ uptake is raw vertically integrated $^{15}NO_3^-$ uptake. $^{15}NO_3^-$ uptake* is a conservative estimate calculated assuming that the *f*-ratio at any depth cannot exceed 1. Thorium is calculated from the steady-state ^{234}Th deficiency model and sediment trap C:^{234}Th ratios. Error bars are standard deviations of replicate measurements.

Regardless of the export method used for comparison, gravitational flux was significantly less than the regionally averaged nitrate uptake rates (mean for CRD cycles = 8.6 ± 6.1 mmol N m^{-2} day^{-1}, range 4.8–17.7, Fig. 6). Even using conservative uptake measurements, nitrate uptake estimates were always significantly greater than contemporaneous measurements of export by sediment traps or ^{234}Th (Fig. 6, Table III). Conservative nitrate uptake averaged 4.8 ± 2.1 mmol N m^{-2} day^{-1}, exceeding shallow trap PN export by a factor of 5.7–8.9 ($P = 0.023$) and ^{234}Th-based flux estimates by a factor of 4.8–9.3 ($P = 0.019$). Cycle 1 (coastal) was the only cycle for which nitrate uptake was near balance with export, with a nitrate uptake rate of 3.0 ± 0.5 mmol N m^{-2} day^{-1} compared with shallow sediment trap flux of 0.90 ± 0.11 mmol N m^{-2} day^{-1} and ^{234}Th-derived flux of 2.6 ± 0.8 mg N m^{-2} day^{-1} (Fig. 6).

DISCUSSION

Methodological uncertainties in export and new production

The steady-state approximation used to estimate open-ocean export by ^{238}U:^{234}Th has potential uncertainties associated with short-term (week to month) changes in ^{234}Th concentrations and the vertical introduction of ^{234}Th to surface water. A full budget for water column ^{234}Th activity can be written as

$$\frac{\partial^{234}\mathrm{Th}}{\partial t} = (^{238}U - ^{234}\mathrm{Th})\lambda_{234} - E + V \qquad (1)$$

where ^{234}Th and ^{238}U are the activities of the respective isotopes, λ_{234} is the ^{234}Th decay constant, E is ^{234}Th export on sinking particles and V is the net advective and diffusive inputs of ^{234}Th into the upper water column (Savoye *et al.*, 2006).

Our Lagrangian sampling scheme, with ^{234}Th measurements made on Days 1 and 4 of the cycles, allows a unique opportunity to test the steady-state assumption for Cycles 2–5. We can calculate the $\delta^{234}\mathrm{Th}/\delta t$ term in Equation (2) (integrated over the upper 90 m) as 1306 ± 1664, −8831 ± 1774, 4743 ± 1366 and −623 ± 2041 dpm m^{-2} day^{-1} for Cycles 2–5, respectively. Therefore, with no statistically significant change for two cycles and one cycle each with increasing or decreasing concentrations, there is no clear region-wide trend of increasing or decreasing ^{234}Th concentrations. We caution against inferring too much from these results; however, as the strong stratification of the upper water column suggests that our Lagrangian array (drogued at 15 m) would have tracked only the upper water column; hence, changes in the deeper portions of the profiles may have been due to horizontal translation rather than changes with time (particularly given the short duration of the cycles; mean time between ^{234}Th casts = 3.6 days). If, instead, we use the four profiles generated in the core of the dome (Cycle 4 was initiated at a site marked by a drifter left after Cycle 2), we can regress the integrated ^{234}Th against time for these four points (spanning 15 days) to calculate a slope that represents $\delta^{234}\mathrm{Th}/\delta t$. Although this slope was positive (797 ± 1450), suggesting net accumulation of ^{234}Th in the water column, it was not statistically different from zero. It thus seems unlikely that ^{234}Th concentrations decreased systematically throughout the region (i.e. negative $\delta^{234}\mathrm{Th}/\delta t$) to cause a substantial underestimate of our ^{234}Th-based export fluxes.

An underestimate of export can also be derived by not including upwelling in our analyses, which may be substantial in the CRD during some periods. On the basis of nitrate uptake rates and nitrate profiles (see vertical fluxes and the biogeochemistry of the CRD section below), we estimate a steady-state upwelling rate of 0.13 m day^{-1} during our cruise. From this upwelling rate and our measured average vertical derivative of ^{234}Th over the upper 150 m (9.3 ± 2.5 dpm m^{-3} m^{-1}), upwelling would have introduced an additional 108 ± 28 dpm m^{-2} day^{-1} into

Table III: Comparison of measured and estimated nitrogen fluxes (μmol N m^{-2} day^{-1})

Cycle	Region	Dates	Nitrate uptake	Nitrification	Export at 90/100 m (Th)	Export at 90/100 m (SedTrap)	Remin below 50 m	PN accumulation	Mesozoo active transport	Mesozoo biomass production
1	Coastal	June 23–26	2990 ± 525		2572 (86%)	896 ± 105 (30%)	0 (0%)	−7639 (−255%)	<32 ± 74 (<1%)	973 ± 198 (33%)
2	CRD Core	July 3–7	5813 ± 2691	69 ± 20 (1%)	1206 ± 629 (21%)	528 ± 111 (9%)	82 (1%)	5402 (93%)	<68 ± 34 (<1%)	502 ± 37 (9%)
3	CRD Edge	July 8–12	3051 ± 866	8 ± 1 (0%)	371 ± 376 (12%)	551 ± 48 (18%)	143 (5%)	−1869 (−61%)	<323 ± 209 (<11%)	2075 ± 429 (68%)
4	CRD Core	July 14–18	3098 ± 477	19 ± 1 (1%)	370 ± 113 (12%)	404 ± 44 (13%)	64 (2%)	−2787 (−90%)	<82 ± 32 (<3%)	864 ± 149 (28%)
5	CRD Edge	July 19–23	7198 ± 1839		772 ± 75 (11%)	637 ± 74 (9%)	48 (1%)	2810 (39%)	<341 ± 125 (<5%)	1931 ± 168 (27%)
2 and 4	CRD Core	July 3–18	4456 ± 814	44 ± 10 (1%)	591 ± 251 (13%)	489 ± 93 (11%)	83 (2%)	−1335 (−30%)	<75 ± 31 (<2%)	713 ± 92 (16%)
2–5	CRD	Mean	4790 ± 2060	32 ± 33 (1%)	680 ± 399 (14%)	530 ± 96 (11%)	84 (2%)	889 (19%)	<203 ± 149 (<4%)	1343 ± 779 (28%)

Values in parentheses are the percentage of nitrate uptake. Mean ± standard deviation of repeat measurements are given when possible. Columns are: (1) cycle (Cycles 2 and 4 show results from an extended Lagrangian study during which a drifter left at the end of Cycle 2 was revisited for Cycle 4; final row is the mean of Cycles 2–5 in the CRD region), (2) region, (3) Dates, (4) vertically integrated conservative $^{15}NO_3^-$ uptake (e.g. *f*-ratio capped at 1, see nitrate uptake sections in Methods and Results), (5) vertically integrated euphotic zone nitrification (Buchwald *et al.*, in revision). (6) ^{234}Th-derived export, (7) sediment trap-derived export, (8) estimated remineralization between 50-m depth horizon (average depth of euphotic zone) and export measurement horizon (90 or 100 m) as assessed by ^{234}Th deficiency and an estimated rate of change of N:^{234}Th with depth (see Discussion), (9) vertically integrated particulate nitrogen accumulation above the depth horizon used for export determined from samples taken at beginning and end of each cycle. Negative values indicate that PN concentrations were decreasing, thus exacerbating measured imbalances between new and export production (note that no standard deviation is given for these estimates because we could not quantify the portion of uncertainty associated with small errors in tracking a water parcel with our Lagrangian drift array), (10) mesozooplankton active transport estimated from day–night differences in grazing rate (see Décima *et al.*, 2016) and assumptions about the fraction of ingested N that is excreted. Note that, since we estimated that half of all excretion occurred at depth despite the temperature-dependence of mesozooplankton excretion, this is necessarily an overestimate of active transport (see Discussion). (11) Mesozooplankton biomass production (and hence potential export to higher trophic levels, see Discussion).

the upper 90 m of the water column. True ^{234}Th export rates may thus have been ~10% higher than calculated neglecting upwelling.

Export estimates determined from the 1D steady-state approximation agreed well with measured ^{234}Th flux into the drifting sediment traps at both 90 and 150 m (Supplementary data, Fig. S5). For most cycles, paired trap and steady-state ^{234}Th measurements agreed within 1 standard deviation. Direct comparisons of the ratio of the trap-derived ^{234}Th flux to the water column/steady-state ^{234}Th flux measurements suggest that traps measure consistently higher ^{234}Th fluxes than determined from the water column deficiency (19% over-collection based on geometric mean,). While this may suggest that the traps "over-collect" sinking material (e.g. Buesseler, 1991), given the uncertainties in the steady-state model used to determine ^{234}Th fluxes discussed above, we cannot definitively assess sediment trap accuracy. Nevertheless, the relatively close agreement between our two independent estimates of vertical flux suggests that the low export rates measured on this cruise were indicative of water column conditions.

Both methods of measuring export likely underestimate the sinking flux contributions mediated by organisms at trophic levels higher than mesozooplankton. Our sediment traps included a baffle constructed of smaller tubes (12.7-mm inner diameter) that would have led to a negative bias against >1 cm sinking material. Furthermore, although ^{238}U:^{234}Th disequilibrium is typically assumed to measure all gravitational flux, the remarkably high C:^{234}Th ratios of mesozooplankton measured in this study and others (Coale, 1990; Passow *et al.*, 2006) suggest that higher trophic levels (fish, whales, seabirds etc.) should ingest negligible ^{234}Th and hence be essentially invisible to the ^{234}Th method.

Shallow water nitrification can also lead to overestimates of new production, if those rates are significant relative to new nitrate delivery to the euphotic zone by physical mechanisms (Dore and Karl, 1996; Yool *et al.*, 2007). Experiments on our cruise (Buchwald *et al.*, in revision) measured euphotic zone nitrification rates of up to 2 nmol L^{-1} day^{-1} (typically an order of magnitude lower). Even assuming this upper limit, however, it is clear that upwelling must supply most of the nitrate uptake (~100 nmol L^{-1} day^{-1}) by the phytoplankton community. Additionally, our estimate of new production could be low since we did not include N_2 fixation, which has been shown to play a significant role in the nitrogen cycle above the OMZ in other portions of the ETP (White *et al.*, 2013). However, $\delta^{15}N$ measurements of suspended PN do not show the surface depletion of ^{15}N that would be expected if N_2 fixation rates were significant during our cruise (N_2 has $\delta_{15}N$ ~0), but rather reflect the

deep-water nitrate signature ($\delta^{15}N_{NO3-}$ ~7) at the base of the euphotic zone.

Trace metal contamination could have potentially caused an overestimate of nitrate uptake, since our samples were not taken from a trace metal clean rosette. Nutrient amendment experiments on our cruise showed co-limitation of phytoplankton by Si and Zn or Fe (Chappell *et al.*, 2016). Furthermore, other samples taken from the non-trace metal rosette showed increases in cellular Chl *a* during 24-h *in situ* incubations that are consistent with trace metal contamination (Selph *et al.*, 2016). However, our 24-h incubations showed no enhancement in nitrate uptake relative to simultaneous 4-h incubations (Fig. 3), suggesting that if trace metal enhancement of nitrate uptake occurred, it must have initiated rapidly.

The balance of new and export production

The large imbalance between new production (nitrate uptake) and export (gravitational flux measured by sediment traps and ^{234}Th) warrants further discussion. Such an imbalance can result from three scenarios: (i) temporal decoupling, (ii) spatial decoupling and (iii) food web and physical processes other than sinking that remove C and N from the surface ecosystem (Fig. 7). While the first two scenarios reflect the spatiotemporal variability of pelagic processes, the third can be restated as a distinct hypothesis: gravitational particle flux is not the dominant process responsible for removing POM from the CRD surface layer during our sampling period. In this section, we will discuss the likelihood of each of these scenarios contributing to the measured imbalance and compare the potential magnitudes of various mechanisms that could reconcile the imbalance including shallow remineralization, PN accumulation in the surface layer, active transport by diel vertically migrating (DVM) mesozooplankton and passive flux of DON to depth. We will also comment on evidence for this imbalance in other marine ecosystems.

Temporal variability in physical upwelling rates can lead to imbalances between new and export production if enhanced nutrient supply leads to periods of excess production and biomass accumulation followed by periods of excess export during the relaxation of upwelling. We cannot entirely rule out such a scenario without longer term (e.g. greater than weekly sampling frequency across a wide region for a period of at least several months). However, testable predictions can be made about food web and physical processes based on this temporal decoupling scenario (Fig. 7A). For instance, during temporal pulses of upwelling and new production, we would expect thermocline shoaling and increased surface

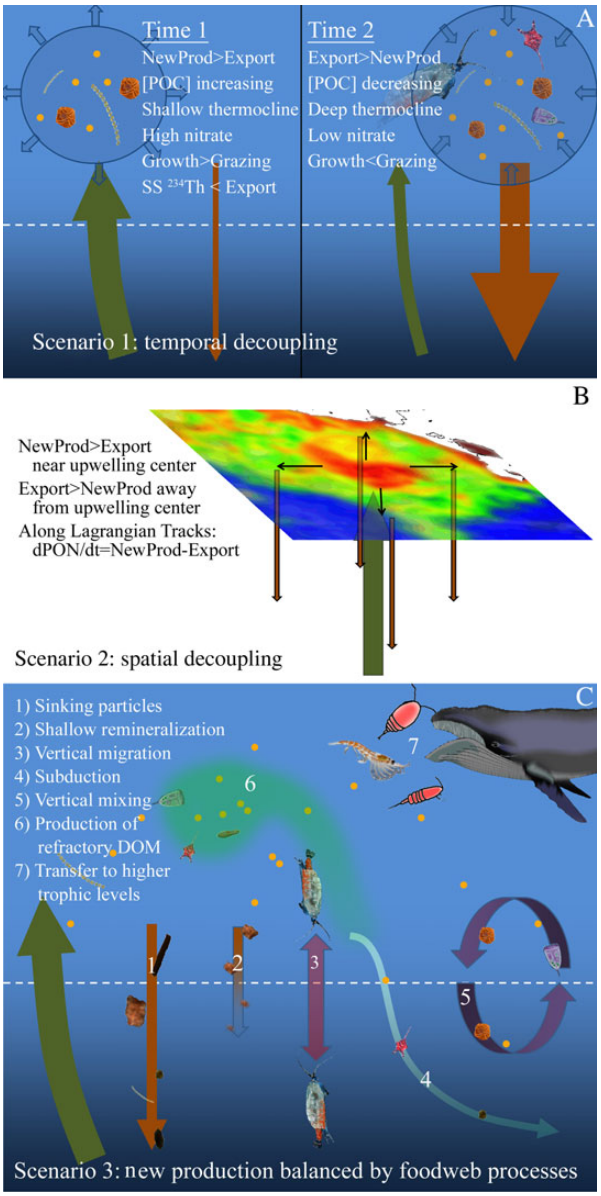

Figure 7. Schematic diagram showing potential reasons for a deficit of sinking particle export relative to new production. Panel **A** shows temporal decoupling with the initial (excess new production) condition shown on the left and the subsequent (excess export) condition shown on the right. Panel **B** shows spatial decoupling at an open-ocean upwelling location. Panel **C** shows food web and physical transport processes that can lead to additional N export that would not be measured by sediment traps or ^{234}Th.

nutrient concentrations relative to the climatological mean. However, during our cruise, the 24°C isotherm was depressed relative to summer mean values (Fiedler and Talley, 2006) and surface nitrate concentrations (0.5−1.7 μmol L^{-1} for Cycles 2−5) were lower than measured on a previous summer cruise in the region (Saito *et al.*, 2005). Furthermore, pulses of new production

should coincide with periods of POM buildup and excess phytoplankton growth relative to grazing. However, during our extended Lagrangian experiment in the core of the dome (including Cycles 2 and 4), PN declined by 20 mmol N m^{-2} day^{-1} over a 15-day period (Table III), and Chl *a*-based grazing estimates (protozoans + mesozooplankton) actually exceeded concurrent phytoplankton growth rate measurements when averaged over the CRD cycles on our cruise (although the difference was not statistically significant, Landry *et al.*, 2016a). During active upwelling, we would also predict that the physical delivery of ^{234}Th into surface waters would result in our simple steady-state (without upwelling-correction) ^{234}Th export equation underestimating total ^{234}Th vertical fluxes. However, Cycles 2 and 4 (in the dome core) showed no such trend, with Cycle 2 suggesting a slight overestimate by the steady-state equation and Cycle 4 a slight underestimate (Supplementary data, Fig. S5). Thus, the available evidence (aside from the excess new production) does not conform to expectations for a temporary period of increased upwelling and new production, but more accurately matches what would be expected for the second time period of Fig. 7A when upwelling has relaxed and biomass is decreasing. Although it is impossible to rule out the possibility that gravitational flux would have increased (by a factor of 6 or higher) at some indeterminate time after our cruise, it seems more likely that the system was in a transient steady-state in which new production in the core of the dome is balanced not by sinking particle flux, but instead by other forms of export.

Spatial decoupling (Fig. 7B) can also separate new production from export if lateral advection drives net advection of organic matter from the upwelling center. This mechanism would lead to excess new production near the site of maximum upwelling and net export somewhere downstream. However, across our five cycles, we found no evidence of regions with enhanced export production. This certainly does not exclude the possibility that excess export would be found elsewhere in the region (the currents surrounding the CRD are complex and it is difficult to assess the spatial scales over which mass balance should be expected). Nonetheless, when considered in a Lagrangian framework, the spatial decoupling mechanism would also predict that short-term imbalances between new and export production would result in biomass accumulation: New production = net biomass accumulation + export. We tested this possibility by comparing vertically integrated (surface to 80–100 m) PN at the beginning and end of our 4-day Lagrangian cycles. While this approach involves some uncertainty (estimates of biomass accumulation are determined from only two PN profiles, and deep layers move relative to our mixed-layer drogued drift array), we found no consistent PN accumulation trend. On Cycles 1, 3 and 4, PN concentrations actually declined at rates of −7.6, −1.9 and −2.9 mmol N m^{-2} day^{-1}, respectively. Cycles 2 and 5 showed PN accumulation at rates of 5.4 and 2.8 mmol N m^{-2} day^{-1}, respectively. If we look at the combined 15-day Lagrangian study in the dome core (Cycles 2 and 4), PN decreased at a rate of 1.3 mmol N m^{-2} day^{-1}. Although cycle PN accumulation rates were only sufficient to close the discrepancy between new and export production for Cycle 2, it is interesting to note that higher (positive) PN accumulation was typically found during the cycles with greater imbalance of new and export production estimates (Table III). Combined, these results demonstrate that the Lagrangian study design allowed us to assess the impact of non-steady-state conditions on the balance of new and export production, and that our region-wide measured excess of new production cannot be solely (or even primarily) explained by short-term biomass increase or spatial decoupling. Rather, it seems likely that other food web processes or physically driven vertical transport mechanisms are responsible for N export out of the CRD surface ecosystem (Fig. 7C). Below, we address shallow remineralization, mesozooplankton vertical migration, mesozooplankton-mediated N transport to higher trophic levels, production of refractory DOM, subduction and vertical mixing as potential reasons that gravitational flux is substantially less than new production during our study.

Our shallow sediment traps were deployed at a depth of 90–100 m, but ^{14}C-PP was typically restricted to the upper 50 m of the water column. To determine whether rapid shallow remineralization between 50 and 90 m could have been responsible for the ~6-fold difference between new production and export, we analyzed our ^{234}Th deficiency profiles, which showed insubstantial remineralization of ^{234}Th between 50 and 100 m. Since C and N remineralization can occur without simultaneous net remineralization of ^{234}Th, we also estimated the change in C:^{234}Th ratios with depth (Supplementary data, Fig. S6). We have a total of nine measurement pairs (four *in situ* pump, five sediment trap) for which we have measurements of C:^{234}Th made at different depths on the same cycle, using the same method. From these paired measurements, the harmonic mean change of C:^{234}Th with depth is −18 nmol C dpm^{-1} m^{-1}. With this information, combined with the C:^{234}Th ratio of the shallowest sediment trap deployment and vertical profiles of ^{234}Th, we can estimate vertical flux at 50 m and hence the amount of remineralization immediately below the euphotic zone. On the basis of this approach, remineralization rates from 50 m to the depth of the shallowest sediment trap varied from 7 to 20%, with a mean across

CRD cycles of 14%. While this analysis involves large uncertainty because we cannot fully constrain how C:^{234}Th ratios changed with depth, remineralization rates between 50 and 100 m were significantly less than the >80% remineralization that would be needed to close the imbalance between new and export production (Table III).

Another mechanism for generating an imbalance between new production and sinking particle flux is active transport by DVM mesozooplankton that feed in the surface and respire at depth (Steinberg *et al.*, 2000; Hannides *et al.*, 2009; Stukel *et al.*, 2013b). Across the CRD, grazing measurements of DVM mesozooplankton averaged 1.11 mg Chl *a* m^{-2} day^{-1} as determined by differences in day–night gut pigment measurements (Décima *et al.*, 2016). If we apply the euphotic zone-weighted average C:Chl ratio of 73 μg C: μg Chl calculated for the FLUZiE cruise by Stukel *et al.* (Stukel *et al.*, 2013a), this would equate to a grazing rate by DVM zooplankton of 1.02 mmol N m^{-2} day^{-1}. Only a fraction of the nitrogen consumed by these mesozooplankton will actually be transported to depth. Defecation by mesozooplankton typically averages 30% of consumption (Conover, 1966), while biomass production averages another 30% (Straile, 1997). Excretion and respiration are thus likely capped at a sum of ~40% of ingestion. If we assume that half of this excretion occurs beneath the euphotic zone (likely an overestimate because specific respiration typically decreases with temperature and the CRD features a strong thermocline), we can calculate an upper estimate of nitrogen transport mediated by the excretion of DVM mesozooplankton of 0.2 mmol N m^{-2} day^{-1} (with a likely Q_{10} of ~2 and temperature changes of >10°C across the thermocline, it is more likely that less than one-third of total respiration of DVM mesozooplankton occurred at depth). While this is a substantial C and N transport (equivalent to 38% of our shallow sediment trap-derived flux), it does not close the large imbalance between new and export production.

In addition to the transport of C and N to depth, mesozooplankton can also remove biomass from the ecosystem by incorporating it into their own biomass where it can be stored over the lifetime of the organism or passed to higher trophic levels. We can estimate this potential export mechanism from mesozooplankton grazing rate measurements (4.9 mg Chl *a* m^{-2} day^{-1}, Décima *et al.*, 2016) and gross growth efficiencies (typical GGE = 0.3, Straile, 1997). With this approach, we find that mesozooplankton may remove an additional 1.3 mmol N m^{-2} day^{-1} from the ecosystem (28% of new production, Table III). While this analysis neglects potential additional production of mesozooplankton based on the consumption of protozoans (a negative bias), it also neglects respiration by higher trophic levels (a positive bias). The fate of this biomass production (predation by fish or squid in the meso- or epipelagic, mortality and sinking of the carcasses, grazing by migratory cetaceans or seabirds, egg production) cannot be determined from the present data. We note, however, that net tows on our cruise sampled abundant gelatinous zooplankton (salps and pyrosomes), which feed predominantly on basal trophic levels, but have few predators. Hence, they have been found to contribute substantially to export flux when their carcasses sink (Smith *et al.*, 2014). Many of the aforementioned mechanisms can lead to export of material from the CRD surface ecosystem without contributing to the sinking flux signal measured by sediment traps or ^{234}Th (e.g. migratory porpoises can transport production laterally, sinking salp carcasses and fish fecal pellets will not be quantitatively sampled by our sediment traps and have a very high C:^{234}Th ratio).

Another mechanism that has been suggested to transport organic carbon and nitrogen to depth is the DOM pump (Carlson *et al.*, 1994). The DOM pump is driven by the production of DOC and DON by plankton at the surface and its conversion by biotic and abiotic processes to refractory forms that cannot be readily utilized by microbial communities. This refractory component of the DOM pool then survives degradation long enough to be transported to depth by subduction or mixing processes. Unfortunately, we lack DOM measurements for this cruise, and hence cannot directly assess the potential impact of this mechanism. Nonetheless, in the open-ocean upwelling system of the Equatorial Pacific, the DOM pump was found to contribute only a minor amount of total carbon export (Carlson and Ducklow, 1995; Quay, 1997). Given the high stratification and typically upwelling conditions in the CRD euphotic zone, it seems unlikely that the DOM pump would be responsible for a substantial fraction of total export, unless there is strong lateral transport of significant DOM out of our sampling area. Similarly, subduction and vertical mixing of POM would not be expected to contribute substantially to vertical N flux in a stratified upwelling region. However, Kessler (Kessler, 2006) noted that upwelling transport in the CRD must be balanced by downward diffusion of heat; thus, it is possible that such mixing (whether along or across isopycnals) may transport POM and DOM to depth.

While the low export rates (relative to nitrate uptake) measured in this study would not have been expected based on the hypothesis proposed by Eppley and Peterson (Eppley and Peterson, 1979), they are actually consistent with the results found in nearby ecosystems. In the Equatorial Pacific, for example, results from the JGOFS EqPac study suggested region-wide export ratios

ranging from <0.05 to 0.10 (Buesseler *et al.*, 1995), while nitrate uptake measurements suggested an *f*-ratio of 0.14 (McCarthy *et al.*, 1996). More recent measurements of nitrate uptake in the Equatorial Pacific indicate an even higher *f*-ratio of 0.26 (Parker *et al.*, 2011), which is similar to our measurements in the CRD. Simultaneous export and nitrate uptake measurements made during time-series studies at the equator also showed significant net new production relative to export (Bacon *et al.*, 1996). Within the southern California Current Ecosystem, Stukel *et al.* (Stukel *et al.*, 2011) found a surplus of new production in coastal waters, while Munro *et al.* (Munro *et al.*, 2013) measured net community production rates that are higher than typical export rates in the region (Stukel *et al.*, 2013b).

In other regions, a focused season-long study in the Western Antarctic Peninsula found an imbalance between nitrate uptake, nitrate drawdown and net community production (all high), and vertical nitrogen flux estimated by sediment traps or ^{234}Th:^{238}U disequilibria, both of which were a factor of 6 lower than nitrate uptake (Stukel *et al.*, 2015). In the Sargasso Sea, a 2-year study found *f*-ratios of 0.39 and 0.08 for the years 1992 and 1993, when sediment trap *e*-ratios were only 0.04 and 0.06, respectively (Lipschultz, 2001; Steinberg *et al.*, 2001), and studies during late-winter storms suggested that export was <35% of nitrate uptake (Maiti *et al.*, 2009). Emerson (Emerson, 2014) suggested that vertically migrating zooplankton may help to close a gap between net community production and sinking flux at the Hawaii Ocean Time-series site and Ocean Station Papa, but they were insufficient to close the imbalance in the Sargasso Sea. In the JGOFS Arabian Sea Program, *f*-ratios also exceeded thorium-derived export ratios by roughly a factor of 2 (Buesseler *et al.*, 1998; Sambrotto, 2001). It thus seems that, across large ocean regions, excess new production over measured gravitational export may be a common biogeochemical occurrence, with different mechanisms (e.g. DVM mesozooplankton, DOM pump, lateral advection, export to higher trophic levels and advective and diffusive transport to depth) potentially responsible for closing the imbalance in each region (Burd *et al.*, 2010).

Vertical fluxes and the biogeochemistry of the CRD

The CRD is an understudied, productive feature in the ETP. It overlies one of the largest OMZs in the world ocean and also contains the highest recorded concentrations of *Synechococcus* (Li *et al.*, 1983; Saito *et al.*, 2005). Surprisingly, for a picophytoplankton-dominated community (but common for other open-ocean upwelling regions), the CRD also supports high biomasses of whales and other higher trophic levels (Reilly and Thayer, 1990; Vilchis *et al.*, 2006).

Our results suggest that the CRD is a region with high nitrate uptake rates, but low vertical fluxes of carbon, nitrogen and phosphorus. Nitrate uptake in the region seems to be driven more by the activities of nano- and micro-phytoplankton than by the abundant picophytoplankton in the region, based on correlations between nitrate uptake and the production of each size class (Supplementary data, Fig. S2). This conclusion agrees with independent results from our cruise of Krause *et al.* (2016) who found that diatoms, despite low biomass, were disproportionately responsible for nitrate uptake and carbon export, and Landry *et al.* (2016b), who found that larger phytoplankton had a disproportionately important role in production compared with their biomass contribution.

Our nitrate uptake rates in the CRD are similar to (but slightly higher than) measurements in an adjacent open-ocean upwelling region, the Eastern Equatorial Pacific (Parker *et al.*, 2011). Our mean conservative nitrate uptake rate for the upper 50 m of four offshore cycles (4.2 mmol N m^{-2} day^{-1}), combined with the mean gradient in nitrate over the upper 50 m of the water column (0.66 mmol N m^{-3} m^{-1}), suggests that only a moderate mean areal upwelling rate of 0.13 m day^{-1} is necessary to provide the nitrate required by the phytoplankton community. It is important to note, however, that this 1D calculation oversimplifies nutrient delivery dynamics that are certainly heterogeneous in time and space.

The low export rates measured for this picoplankton-dominated region are consistent with the traditional paradigm that highlights the importance of diatoms and other large phytoplankton in POM vertical fluxes (Michaels and Silver, 1988). Nonetheless, despite suppressed diatom biomass in the CRD, low export is surprising for a productive ecosystem with high zooplankton biomass situated above an OMZ. The latter seems to be more a matter of accumulated POM decomposition over time as the subsurface water makes its way to the region, but it is reinforced by the strong CRD thermocline, which minimizes vertical mixing and ventilation. High grazing rates of mesozooplankton in the CRD (Décima *et al.*, 2016), combined with higher than expected remineralization rates of their fecal pellets in the euphotic zone (Stukel *et al.*, 2013a), suggest that mesozooplankton play a key role in shunting new production to higher trophic levels rather than to the vertical POM flux pathways that seem to dominate export production in other productive ecosystems. However, more studies need to be conducted before we can extrapolate from these results (determined during a mild El Niño) to the average behavior of this dynamic ecosystem.

SUPPLEMENTARY DATA

Supplementary data can be found online at http://plankt.oxfordjournals.org.

DATA ARCHIVING

Core data from this manuscript (nitrate uptake, sediment trap and ^{234}Th) is available from the Biological and Chemical Oceanography Data Management Office (http://www.bco-dmo.org/).

ACKNOWLEDGMENTS

This manuscript would not have been possible without the support of many friends and collaborators on the FLUZiE cruise. We particularly thank Darcy Taniguchi, Karen Selph, Alain de Verneil, Dan Wick, John Wokuluk, Joaquim Goes and Jim Moffett. We also thank the wonderful captain, crew and research technicians of the R/V Melville, who did an excellent job in facilitating our research goals. We also thank our Associate Editor and three anonymous reviewers for their insightful comments.

FUNDING

This study was supported by U. S. National Science Foundation grant (OCE-0826626 to M.R.L.). Additional support was provided by a National Aeronautics and Space Administration, Earth and Space Science Fellowship to M.R.S.

REFERENCES

Aspila, K. I., Agemian, H. and Chau, A. S. Y. (1976) A semi-automated method for determination of inorganic, organic and total phosphate in sediments. *Analyst*, **101**, 187–197.

Bacon, M. P., Cochran, J. K., Hirschberg, D., Hammar, T. R. and Fleer, A. P. (1996) Export flux of carbon at the equator during the EqPac time-series cruises estimated from Th-234 measurements. *Deep Sea Res. Part II*, **43**, 1133–1153.

Benitez-Nelson, C. R., Buesseler, K. O., Van Der Loeff, M. R., Andrews, J., Ball, L., Crossin, G. and Charette, M. A. (2001) Testing a new small-volume technique for determining Th-234 in seawater. *J. Radioanal. Nucl. Chem.*, **248**, 795–799.

Benitez-Nelson, C. R., Madden, L. P. O., Styles, R. M., Thunell, R. C. and Astor, Y. (2007) Inorganic and organic sinking particulate phosphorus fluxes across the oxic/anoxic water column of Cariaco Basin, Venezuela. *Mar. Chem.*, **105**, 90–100.

Buchwald, C., Santoro, A. E., Stanley, H. R. and Casciotti, K. L. (in revision) Nitrogen cycling in the secondary nitrite maximum in the Costa Rica Upwelling Dome. *Global Biogeochem. Cycles*.

Buesseler, K., Ball, L., Andrews, J., Benitez-Nelson, C., Belastock, R., Chai, F. and Chao, Y. (1998) Upper ocean export of particulate organic carbon in the Arabian Sea derived from thorium-234. *Deep Sea Res. II*, **45**, 2461–2487.

Buesseler, K. O. (1991) Do upper-ocean sediment traps provide an accurate record of particle flux? *Nature*, **353**, 420–423.

Buesseler, K. O., Andrews, J. A., Hartman, M. C., Belastock, R. and Chai, F. (1995) Regional estimates of the export flux of particulate organic carbon derived from thorium-234 during the JGOFS EqPac Program. *Deep Sea Res. II*, **42**, 777–804.

Buesseler, K. O., Benitez-Nelson, C., Van Der Loeff, M. R., Andrews, J., Ball, L., Crossin, G. and Charette, M. A. (2001) An intercomparison of small- and large-volume techniques for thorium-234 in seawater. *Mar. Chem.*, **74**, 15–28.

Burd, A. B., Hansell, D. A., Steinberg, D. K., Anderson, T. R., Aristegui, J., Baltar, F., Beaupre, S. R., Buesseler, K. O. *et al.* (2010) Assessing the apparent imbalance between geochemical and biochemical indicators of meso- and bathypelagic biological activity: what the @$#! is wrong with present calculations of carbon budgets? *Deep Sea Res. II*, **57**, 1557–1571.

Carlson, C. A. and Ducklow, H. W. (1995) Dissolved organic carbon in the upper ocean of the central Equatorial Pacific Ocean, 1992: daily and finescale vertical variations. *Deep Sea Res. II*, **42**, 639–656.

Carlson, C. A., Ducklow, H. W. and Michaels, A. F. (1994) Annual flux of dissolved organic carbon from the euphotic zone in the northwestern Sargasso Sea. *Nature*, **371**, 405–408.

Chappell, P. D., Vedamati, J., Selph, K. E., Cyr, H. A., Jenkins, B. D., Landry, M. R. and Moffett, J. W. (2016) Preferential depletion of zinc within Costa Rica Upwelling Dome creates conditions for zinc co-limitation of primary production. *J. Plankton Res.*, **38**, 244–255.

Coale, K. H. (1990) Labyrinth of doom: a device to minimize the swimmer component in sediment trap collections. *Limnol. Oceanogr.*, **35**, 1376–1381.

Conover, R. J. (1966) Assimilation of organic matter by zooplankton. *Limnol. Oceanogr.*, **11**, 338–345.

Décima, M., Landry, M. R., Stukel, M. R., Lopez-Lopez, L. and Krause, J. W. (2016) Mesozooplankton biomass and grazing in the Costa Rica Dome: amplifying variability through the plankton food web. *J. Plankton Res.*, **38**, 317–330.

Dore, J. E. and Karl, D. M. (1996) Nitrification in the euphotic zone as a source for nitrite, nitrate, and nitrous oxide at Station ALOHA. *Limnol. Oceanogr.*, **41**, 1619–1628.

Dugdale, R. C. and Wilkerson, F. P. (1986) The use of N-15 to measure nitrogen uptake in eutrophic oceans: experimental considerations. *Limnol. Oceanogr.*, **31**, 673–689.

Emerson, S. (2014) Annual net community production and the biological carbon flux in the ocean. *Global Biogeochem. Cycles*, **28**, 14–28.

Eppley, R. W. and Peterson, B. J. (1979) Particulate organic matter flux and planktonic new production in the deep ocean. *Nature*, **282**, 677–680.

Fernandez-Alamo, M. A. and Farber-Lorda, J. (2006) Zooplankton and the oceanography of the eastern tropical Pacific: a review. *Prog. Oceanogr.*, **69**, 318–359.

Fiedler, P. C. (2002) The annual cycle and biological effects of the Costa Rica Dome. *Deep Sea Res. Part II*, **49**, 321–338.

Fiedler, P. C. and Talley, L. D. (2006) Hydrography of the eastern tropical Pacific: a review. *Prog. Oceanogr.*, **69**, 143–180.

Goes, J. I. and Al, E. (2015) Biological response to silicate and trace metals in the Costa Rica Dome. *J. Plankton Res.*, in preparation.

Hannides, C. C. S., Landry, M. R., Benitez-Nelson, C. R., Styles, R. M., Montoya, J. P. and Karl, D. M. (2009) Export stoichiometry and migrant-mediated flux of phosphorus in the North Pacific Subtropical Gyre. *Deep Sea Res. Part I*, **56**, 73–88.

Hofmann, E. E., Busalacchi, A. J. and Obrien, J. J. (1981) Wind generation of the Costa Rica Dome. *Science*, **214**, 552–554.

Kessler, W. S. (2006) The circulation of the eastern tropical Pacific: a review. *Prog. Oceanogr.*, **69**, 181–217.

Knauer, G. A., Martin, J. H. and Bruland, K. W. (1979) Fluxes of particulate carbon, nitrogen, and phosphorus in the upper water column of the Northeast Pacific. *Deep Sea Res.*, **26**, 97–108.

Krause, J. W., Stukel, M. R., Taylor, A. G., Taniguchi, D. A., De Verneil, A. and Landry, M. R. (2016) Net biogenic silica production and the contribution of diatoms to new production and organic matter export in the Costa Rica Dome ecosystem. *J. Plankton Res.*, **38**, 216–229.

Landry, M. R., Ohman, M. D., Goericke, R., Stukel, M. R. and Tsyrklevich, K. (2009) Lagrangian studies of phytoplankton growth and grazing relationships in a coastal upwelling ecosystem off Southern California. *Prog. Oceanogr.*, **83**, 208–216.

Landry, M. R., De Verneil, A., Goes, J. I. and Moffett, J. W. (2016a) Plankton dynamics and biogeochemical fluxes in the Costa Rica Dome: introduction to CRD Flux and Zinc Experiments. *J. Plankton Res.*, **38**, 167–182.

Landry, M. R., Selph, K. E., Décima, M., Gutierrez-Rodriquez, A., Stukel, M. R., Taylor, A. G. and Pasulka, A. L. (2016b) Phytoplankton production and grazing balances in the Costa Rica Dome. *J. Plankton Res.*, **38**, 366–379.

Li, W. K. W., Rao, D. V. S., Harrison, W. G., Smith, J. C., Cullen, J. J., Irwin, B. and Platt, T. (1983) Autotrophic picoplankton in the tropical ocean. *Science*, **219**, 292–295.

Lipschultz, F. (2001) A time-series assessment of the nitrogen cycle at BATS. *Deep Sea Res. Part II*, **48**, 1897–1924.

Maiti, K., Benitez-Nelson, C. R., Lomas, M. W. and Krause, J. W. (2009) Biogeochemical responses to late-winter storms in the Sargasso Sea, III—estimates of export production using Th-234:U-238 disequilibria and sediment traps. *Deep Sea Res. Part I*, **56**, 875–891.

Mccarthy, J. J., Garside, C., Nevins, J. L. and Barber, R. T. (1996) New production along 140°W in the equatorial Pacific during and following the 1992 El Niño event. *Deep Sea Res. Part II*, **43**, 1065–1093.

Michaels, A. F. and Silver, M. W. (1988) Primary production, sinking fluxes and the microbial food web. *Deep Sea Res.*, **35**, 473–490.

Mulholland, M. R. and Lomas, M. W. (2008) Nitrogen uptake and assimilation. In: Capone, D. G., Bronk, D. A., Mulholland, M. R. and Carpenter, E. J. (eds), *Nitrogen in the Marine Environment*, 2nd ed. Academic Press, Boston, pp. 303–384.

Munro, D. R., Quay, P. D., Juranek, L. W. and Goericke, R. (2013) Biological production rates off the Southern California coast estimated from triple O_2 isotopes and O_2:Ar gas ratios. *Limnol. Oceanogr.*, **58**, 1312–1328.

Murray, J. W., Young, J., Newton, J., Dunne, J., Chapin, T., Paul, B. and Mccarthy, J. J. (1996) Export flux of particulate organic carbon from the central equatorial Pacific determined using a combined drifting trap Th-234 approach. *Deep Sea Res. Part II*, **43**, 1095–1132.

Parker, A. E., Wilkerson, F. P., Dugdale, R. C., Marchi, A. and Hogue, V. (2011) Patterns of nitrogen concentration and uptake by two phytoplankton size-classes in the equatorial Pacific Ocean (110°W–140°W) during 2004 and 2005. *Deep Sea Res. II*, **58**, 417–433.

Passow, U., Dunne, J., Murray, J. W., Balistrieri, L. and Alldredge, A. L. (2006) Organic carbon to Th-234 ratios of marine organic matter. *Mar. Chem.*, **100**, 323–336.

Pike, S. M., Buesseler, K. O., Andrews, J. and Savoye, N. (2005) Quantification of ^{234}Th recovery in small volume sea water samples by inductively coupled plasma-mass spectrometry. *J. Radioanal. Nucl. Chem.*, **263**, 355–360.

Quay, P. (1997) Was a carbon balance measured in the equatorial Pacific during JGOFS? *Deep Sea Res. Part II*, **44**, 1765–1781.

Reilly, S. B. and Thayer, V. G. (1990) Blue whale (*Balaenoptera musculus*) distribution in the Eastern Tropical Pacific. *Mar. Mammal. Sci.*, **6**, 265–277.

Riley, G. A. (1970) Particulate organic matter in sea water. *Advances in Marine Biology*, **8**, 1–118.

Saito, M. A., Rocap, G. and Moffett, J. W. (2005) Production of cobalt binding ligands in a *Synechococcus* feature at the Costa Rica upwelling dome. *Limnol. Oceanogr.*, **50**, 279–290.

Sambrotto, R. N. (2001) Nitrogen production in the northern Arabian Sea during the Spring Intermonsoon and Southwest Monsoon seasons. *Deep Sea Res. Part II*, **48**, 1173–1198.

Savoye, N., Benitez-Nelson, C., Burd, A. B., Cochran, J. K., Charette, M., Buesseler, K. O., Jackson, G. A., Roy-Barman, M. *et al.* (2006) ^{234}Th sorption and export models in the water column: a review. *Mar. Chem.*, **100**, 234–249.

Selph, K. E., Landry, M. R., Taylor, A. G., Gutierrez-Rodriguez, A., Stukel, M. R., Wokuluk, J. and Pasulka, A. (2016) Phytoplankton production and taxon-specific growth rates in the Costa Rica Dome. *J. Plankton Res.*, **38**, 199–215.

Sigman, D. M., Casciotti, K. L., Andreani, M., Barford, C., Galanter, M. and Bohlke, J. K. (2001) A bacterial method for the nitrogen isotopic analysis of nitrate in seawater and freshwater. *Anal. Chem.*, **73**, 4145–4153.

Smith, K. L. Jr, Sherman, A. D., Huffard, C. L., Mcgill, P. R., Henthorn, R., Von Thun, S., Ruhl, H. A., Kahru, M. *et al.* (2014) Large salp bloom export from the upper ocean and benthic community response in the abyssal northeast Pacific: day to week resolution. *Limnol. Oceanogr.*, **59**, 745–757.

Steinberg, D. K., Carlson, C. A., Bates, N. R., Goldthwait, S. A., Madin, L. P. and Michaels, A. F. (2000) Zooplankton vertical migration and the active transport of dissolved organic and inorganic carbon in the Sargasso Sea. *Deep Sea Res. Part I*, **47**, 137–158.

Steinberg, D. K., Carlson, C. A., Bates, N. R., Johnson, R. J., Michaels, A. F. and Knap, A. H. (2001) Overview of the US JGOFS Bermuda Atlantic Time-series Study (BATS): a decade-scale look at ocean biology and biogeochemistry. *Deep Sea Res. Part II*, **48**, 1405–1447.

Straile, D. (1997) Gross growth efficiencies of protozoan and metazoan zooplankton and their dependence on food concentration, predator-prey weight ratio, and taxonomic group. *Limnol. Oceanogr.*, **42**, 1375–1385.

Stukel, M. R., Asher, E., Coutos, N., Schofield, O., Strebel, S., Tortell, P. D. and Ducklow, H. W. (2015) The imbalance of new and export production in the Western Antarctic Peninsula, a potentially "leaky" ecosystem. *Global Biogeochem. Cycles*, **29**, doi:10.1002/2015GB005211.

Stukel, M. R., Décima, M., Selph, K. E., Taniguchi, D. A. A. and Landry, M. R. (2013a) The role of *Synechococcus* in vertical flux in the Costa Rica upwelling dome. *Prog. Oceanogr.*, **112–113**, 49–59.

Stukel, M. R., Landry, M. R., Benitez-Nelson, C. R. and Goericke, R. (2011) Trophic cycling and carbon export relationships in the California Current Ecosystem. *Limnol. Oceanogr.*, **56**, 1866–1878.

Stukel, M. R., Ohman, M. D., Benitez-Nelson, C. R. and Landry, M. R. (2013b) Contributions of mesozooplankton to vertical carbon export in a coastal upwelling system. *Mar. Ecol. Prog. Ser.*, **491**, 47–65.

Van Mooy, B. A. S., Keil, R. G. and Devol, A. H. (2002) Impact of suboxia on sinking particulate organic carbon: enhanced carbon flux and preferential degradation of amino acids via denitrification. *Geochim. Cosmochim. Acta*, **66**, 457–465.

Vilchis, L. I., Ballance, L. T. and Fiedler, P. C. (2006) Pelagic habitat of seabirds in the eastern tropical Pacific: effects of foraging ecology on habitat selection. *Mar. Ecol. Prog. Ser.*, **315**, 279–292.

Wakeham, S. G., Hedges, J. I., Lee, C., Peterson, M. L. and Hernes, P. J. (1997) Compositions and transport of lipid biomarkers through the water column and surficial sediments of the equatorial Pacific Ocean. *Deep Sea Res. Part II*, **44**, 2131–2162.

White, A. E., Foster, R. A., Benitez-Nelson, C. R., Masque, P., Verdeny, E., Popp, B. N., Arthur, K. E. and Prahl, F. G. (2013) Nitrogen fixation in the Gulf of California and the Eastern Tropical North Pacific. *Prog. Oceanogr.*, **109**, 1–17.

Yanada, M. and Maita, Y. (1995) Regional and seasonal variations of biomass and bio-mediated materials in the North Pacific Ocean. In: Sakai, H. and Nozaki, Y. (eds) *Biogeochemical Processes and Ocean Flux in the Western Pacific*. Terra Scientific Publishing Company, Tokyo, pp. 293–306.

Yool, A., Martin, A. P., Fernandez, C. and Clark, D. R. (2007) The significance of nitrification for oceanic new production. *Nature*, **447**, 999–1002.